**Charlton TS, Rouainia M.**

**Probabilistic capacity analysis of suction caissons in spatially variable clay.**

***Computers and Geotechnics* 2016, 80, 226–236.**

# Probabilistic capacity analysis of suction caissons in spatially variable clay

T. S. Charlton[a], M. Rouainia[a]

[a]*Newcastle University, Newcastle upon Tyne NE1 7RU, UK*

**Abstract**

Suction caissons are increasingly used in offshore energy production to moor floating facilities in deep water. The holding capacity of a suction caisson is dependent on the angle of the mooring line and is often described in terms of a vertical-horizontal (VH) load interaction diagram, or failure envelope. These envelopes have commonly been defined by numerical methods using deterministic soil parameters, ignoring the natural spatial variability of seabed sediments. In this paper, spatial variability is modelled using a random field and coupled with finite element analysis to obtain a probabilistic characterisation of holding capacity. The increase of strength with depth that is characteristic of a marine clay is taken into account. A non-parametric approach using kernel density estimation is presented for constructing probabilistic VH failure envelopes that allow an appropriate envelope, associated with an acceptable level of risk, to be selected for design. A study of the autocorrelation distance, a quantity often difficult to obtain accurately in practice, has shown that the vertical autocorrelation distance has a much greater influence on the variability of holding capacity than the horizontal and should be carefully chosen in offshore applications.

*Keywords:* Offshore geotechnics, suction caisson, spatial variability, finite element analysis.

## 1. Introduction

Development of offshore energy resources now regularly occurs in waters exceeding 1000m in depth and the trend towards deep water production has led to much interest in the analysis of anchoring systems [1]. As water depths increase, structures that rest on the seabed and rely on traditional gravity or pile foundations become impractical and moored floating units make greater economic sense. Recently, suction caissons (also known as suction anchors) have received significant attention due to a low cost, accurate and environmentally-friendly installation process, which combines penetration by self-weight and by a pressure differential generated from pumping water out of the caisson.

Once installed, the direction of the load applied to a suction caisson is determined by the mooring arrangement. For catenary moorings, the load is at a shallow angle to the horizontal. In deep water, caissons are increasingly employed in taut-line mooring arrangements where the applied load is either inclined or close to vertical [2]. Knowledge of caisson response under combinations of vertical and horizontal load is therefore required to assess holding capacity.

Zdravkovic et al. [3] used a finite element (FE) method to describe the shape of the vertical-horizontal (VH) load interaction diagrams, or failure envelopes, under various caisson aspect ratios and soil anisotropy. A simple ellipsoidal expression for the VH failure envelopes was presented by Supachawarote et al. [4], again based on FE results. Plastic limit formulations have been developed by Randolph and House [5] and Aubeny et al. [6] to assess capacity under combined VH loading. More recent FE analyses have considered installation effects [7].

However, these studies have all considered a deterministic system in which the mechanical behaviour of the soil is described by parameters assigned a specific value. In reality soil is a naturally complex material, having been formed by a range of physical and chemical processes, and the values of engineering parameters are spatially variable. Uncertainty is therefore an integral part of geotechnical design.

A limited number of studies of the reliability of suction caissons subject to uncertainty in loads and capacity have been undertaken. Clukey et al. [8] considered catenary and taut-leg moorings in which system uncertainty was described in a simplified manner by including random variables, for example undrained shear strength $s_u$, in empirically-derived expressions for lateral and axial capacity. A First-Order Reliability Method (FORM) was used with a linear limit state function to define failure. A design code based on similar analyses has been produced by Dahlberg et al. [9]. A more detailed reliability study has recently been presented by Silva-González et al. [10], with a variety of sources of uncertainty included in a FORM analysis.

Whilst methods such as FORM are useful for quantifying the reliability of a suction caisson at a design point corresponding to a specified limit state function, the spatial variability of the soil is not modelled explicitly and mechanical behaviour is overlooked. Consideration of the spatial variation of soil properties has been shown to affect both capacity and failure mechanisms in a range of geotechnical scenarios such as simple bearing capacity problems and slope failures [e.g. 11, 12].

In this paper, the holding capacity of a suction caisson in a spatially variable undrained clay subjected to combined VH loading is assessed. The increase of strength with depth typical of marine clays is taken into account. Spatial variability is modelled using a random field representation of soil strength parameters. This is coupled with an FE analysis, meaning that the failure mechanism and ultimate capacity is a direct and natural result of the spatial variation of soil parameters. A method for constructing probabilistic VH failure envelopes, allowing the results of the probabilistic capacity analysis to be easily used in design, is demonstrated. Finally a study of the effect of autocorrelation distance, a quantity often difficult to obtain accurately in practice, has been undertaken.

## 2. Computational framework

The computational framework consists of two parts: (a) generation of a random field and (b) an FE analysis of VH capacity. The method is non-intrusive, meaning that the FE solver is treated as a 'black-box' with no modifications to the code. The stochastic response is obtained by Monte Carlo simulation. This involves repeatedly generating a random field and passing the realisation to the deterministic FE solver to calculate the VH capacity.

The non-intrusive scheme is in contrast with intrusive formulations [e.g. 13], where stochastic terms are included in the stiffness matrix. As the FE code is unchanged, powerful commercial software may be used allowing complex geometries and constitutive models to be handled in a straightforward way. All that is required is a mapping of the random field to the FE program. In this paper a stochastic mesh, separate from the FE mesh, is used for this purpose. The random field is discretised into a collection of random variables at the nodes of the stochastic mesh, which consists of bilinear quadrilateral elements. Shape functions are then used to interpolate the values of the random field to the Gauss points of the FE mesh.

### *2.1. Spatial variability of undrained shear strength*

The undrained shear strength, $s_u$, is generally used to determine suction caisson capacity in undrained conditions and therefore in this study the spatial variability of $s_u$ will be considered.

It is convenient to assume that the fluctuations in value of a parameter across a soil mass are randomly occurring. Spatial variability can then be modelled using a random field. To simplify the treatment of random fields an assumption of homogeneity is regularly made, whereby in the case of a Gaussian random the field the mean and variance are constant with depth [14].

In deep water locations, deposition occurs slowly and the typically fine-grained sediments have in general not been subjected to additional vertical stresses. These normally consolidated soils therefore commonly exhibit an increasing shear strength with depth [1]. This creates an additional challenge in simulating spatial variability because the mean, and often the variance, of $s_u$ is not constant across the soil mass and so cannot be modelled using a homogeneous random field. However, the undrained shear strength can be related to the vertical effective stress ($\sigma'_v$) and overconsolidation ratio (OCR) as follows [15]:

$$\frac{s_u}{\sigma'_v} = rOCR^m \tag{1}$$

where $r$ and $m$ are constants. In a normally consolidated soil the OCR is equal to 1, and in this case $r$ is the undrained shear strength ratio ($r = s_u/\sigma'_v$). Accounting for a limited strength at the mudline, $s_{u,m}$:

$$s_u = r\sigma'_v + s_{u,m} = r\gamma' z + s_{u,m} \tag{2}$$

where $\gamma'$ is the effective unit weight and $z$ is the depth below the mudline. Phoon and Kulhawy [22] reported that the typical coefficient of variation (COV) of unit weight is very low, generally less than 0.1. Hence it is reasonable to consider $\gamma'$ as deterministic. Given that $\sigma'_v$ increases with $z$, the variation in the increase of undrained shear strength with depth may be simulated by considering $r$ as a homogeneous random field [16]. Here, $s_{u,m}$ is taken as a deterministic value. The mean ($\mu_{s_u}$) and standard deviation ($\sigma_{s_u}$) of $s_u$ may be written as follows:

$$\mu_{s_u} = s_{u,m} + \gamma' z\mu_r \tag{3}$$

$$\sigma_{s_u} = s_{u,m} + \gamma' z\sigma_r \tag{4}$$

where $\mu_r$ and $\sigma_r$ are respectively the mean and standard deviation of $r$. From Eqs. 3 and 4, it is apparent that both $\mu_{s_u}$ and $\sigma_{s_u}$ are dependent upon the vertical effective stress. The increase in standard deviation of $s_u$ with depth has been observed by Lumb [17] in a normally consolidated marine clay.

*2.2. Generation of random field*

Physically, $s_u$ cannot take a negative value. The ratio $r$ therefore cannot be represented as a Gaussian random field. A lognormal PDF is defined only for values greater than zero and was identified by Lacasse and Nadim ([18] as an appropriate distribution for the undrained shear strength ratio. If $(x, y)$ denotes spatial position, a lognormal random field of $r$ may be generated as follows:

$$r(x, y) = \exp\left[\mu_{L,r} + \sigma_{L,r} G(x, y)\right] \tag{5}$$

And so,

$$s_u(x, y) = s_{u,m} + \gamma' z \exp\left[\mu_{L,r} + \sigma_{L,r} G(x, y)\right] \tag{6}$$

where $\mu_{L,r}$ is the mean of $\ln(r)$, $\sigma_{L,r}$ is the standard deviation of $\ln(r)$ and $G(x, y)$ is a standard homogeneous Gaussian random field of zero mean and unit variance.

Here, the Karhunen-Loeve (KL) expansion is used to produce standard Gaussian random fields. The KL expansion of the zero mean random field $G(x, y)$ is:

$$G(x, y) = \sum_{i=1}^{\infty} \sqrt{\lambda_i} \xi_i \psi_( x, y) \tag{7}$$

where $\psi$ and $\lambda$ are the eigenfunctions and eigenvalues from a spectral decomposition of a prescribed autocorrelation function, $\rho_G$, and $\xi$ is a set of independent standard Gaussian random variables. The infinite sum in Eq. 7 must be truncated in practice and in this study the number of retained terms is chosen so as to capture at least 95% of the variability of $G(x, y)$. An exponential autocorrelation function is used for $\ln(r)$:

$$\rho_G[(x, y), (x', y')] = \exp\left[ -\left(\frac{|x - x'|}{L_x}\right) + \left(\frac{|y - y'|}{L_y}\right)\right] \tag{8}$$

where $L_x$ and $L_y$ are the autocorrelation distances in the $x$- and $y$-directions respectively. Analytical solutions are available for the eigenfunctions and eigenvalues of this autocorrelation function (Ghanem and Spanos, 2003). It is important to note that the autocorrelation distances of $s_u$ are the same as those of $r$ (Wu et al., 2012).

*2.3. Finite element model*

The finite element code Plaxis 2D [25] is used for the deterministic simulations. A plane strain model of a suction caisson was created based on the hypothetical problem analysed by Andresen et al. [20], which in turn was taken from the comprehensive study by Andersen et al. (2005). The layout of the problem is shown in Fig. 1. The caisson has an aspect ratio (L/D) of 1.5 and loading is applied at angles of $\beta$ = 0, 30, 45, 60, 75 and 90$^o$ to produce the VH failure envelope. For each loading case, the load application point (at depth $Z_p$) is chosen so that the line of action passes through the centre of rotation of the caisson ($Z_{cl}$). This leads to a pure translation failure mechanism and an optimal capacity envelope. The location of ($Z_{cl}$) has been studied by Supachawarote et al. (2004), who found that the ratio $Z_{cl}/L$ that results in optimum capacity is around 2/3, and varies only marginally with loading angle. This was reflected in a parametric study undertaken to locate the optimal values of $Z_{cl}$ and $Z_p$ at each loading angle. The same $Z_p$ is used in both deterministic and stochastic simulations, since moving the load application point for each realisation of undrained shear strength would be impractical.

The failure load at each angle is denoted $Q_\beta$, and is composed of horizontal (H) and vertical (V) load components. The uniaxial capacities ($Q_0$ and $Q_{90}$) are referred to as H$^*$ and V$^*$ respectively. Loads from the case of a deterministic profile of $s_u$ are denoted henceforth using the subscript *det.*

The clay is undrained and behaves in a linear elastic-perfectly plastic manner according to the Mohr-Coulomb model with friction angle $\phi' = 0^o$ and cohesion $c = s_u$ (equivalent to the Tresca criterion). The caisson is assumed to act as a rigid body, with the soil plug modelled as a linear elastic material with deterministic properties. Interface elements are applied around the caisson, as shown in Fig. 1. A strength reduction factor of 0.65 is used along the outside walls, as recommended by Andersen and Jostad [26].

Undrained shear strength at the mudline, $s_{u,m}$, is 0.1kPa and $s_u$ increases with depth according to:

$$s_u = 0.1 + 1.25z \tag{9}$$

As $\gamma'$ is taken as 8kN/m$^3$, and referring to Eq. (3), the mean of $r$ is calculated as $\mu_r = 1.25/8 = 0.156$. The coefficient of variance of $r$($COV_r$) is chosen to be 0.2, which is a typical value based on observations of the variability of $s_u$ and the undrained shear strength ratio by Phoon and Kulhawy [22] and Lacasse and Nadim [18].

A domain of size 50m × 20m (10D x 4D) is used to avoid boundary effects. The finite element mesh is shown in Fig. 2 , where boundary conditions are also indicated, and consists of 15-node triangular elements. Monte Carlo simulation requires numerous deterministic runs and consequently a balance must be found between computation time and solution accuracy. A mesh of 4578 nodes was found to overestimate capacity by no more than 1.5% compared to a mesh of over 50,000 nodes whilst the calculation executed significantly faster. This level of discretisation error is seen as acceptable considering the importance that must be given to computation time in stochastic applications. The extremely fine mesh (>50,000 nodes) resulted in a horizontal capacity of 228kN/m, matching that reported by by Andresen et al. [20].

Failure envelopes are presented in normalised form, allowing the plane strain results to be related to the three-dimensional (3D) conditions encountered in practice. Fig. 3 shows the normalised deterministic failure envelope and compares with closed-form expressions derived in other numerical studies, including full 3D FE analyses. Good agreement can be observed between plane strain conditions and the other FE analyses, particularly when the horizontal load component is large. The plane strain model appears to underestimate the normalised capacity when the loading is predominately vertical but the difference is relatively minor and does not affect the main purpose of this study, namely the effect of spatial variability on the failure envelope.

## 3. Results and discussion

The spatial variability of $s_u$ is illustrated in Figs. 4 and 5. Fig. 4 shows the increase of $s_u$ with depth for a vertical cross section of two random field realisations with different vertical autocorrelation distances; the deterministic profile is equivalent to the mean of the stochastic simulations. The increase of $\sigma_{s_u}$ with depth results in greater variability deeper into the clay. The effect of a longer $L_y$ is also clearly seen, with fluctuations around the mean occurring less frequently.

Considering the two-dimensional model, in the deterministic case presented in Fig. 5(a), $s_u$ increases linearly with depth in a uniform manner across the domain, producing horizontal bands of equal strength clay. Fig. 5(b) and 5(c) show realisations of a random field of $s_u$. Zones of weaker and stronger clay occur as the value of $s_u$ fluctuates around the mean. In Fig. 5(b) the autocorrelation is isotropic and relatively short, resulting in localised areas of high and low strength. Fig. 5(c) shows a realisation where the horizontal autocorrelation distance is an order of magnitude greater than the vertical. The fluctuations in $s_u$ can be seen to be less frequent in the horizontal direction.

*3.1. Monte Carlo simulations*

Initially, 1000 simulations were run using an isotropic correlation distance of $L_x = L_y$ =1m. Fig. 6 presents VH failure envelopes for each of the 1000 simulations. Stochastic loads are normalised by the uniaxial deterministic capacities ($V^*_{det}$ and $H^*_{det}$) and the deterministic failure envelope is also shown. The general shape of the envelope is maintained when the spatial variation of the undrained shear strength is considered although 'crossing over' of the failure envelopes does occur, particularly at a loading angle of $45^o$ when the interaction of V and H loading begins to affect horizontal capacity (i.e. $H < H^*$). Depending on load inclination, the difference between deterministic and stochastic capacity may be as much as ± 15%. It is worth repeating that this is solely due to fluctuation of undrained shear strength around a defined trend, the natural scenario in the field.

$$\mu_{Q_\beta} = \frac{1}{n}\sum_{i=1}^{n} Q_{\beta,i} \tag{10}$$

$$\sigma_{Q_\beta} = \sqrt{\frac{1}{n-1}\sum_{i=1}^{n}\left(Q_{\beta,i} - \mu_{Q_\beta}\right)^2} \tag{11}$$

where $n$ is the number of simulations, $Q_{\beta,i}$ refers to the ultimate load in the *i-th* simulation and $\mathrm{COV}_{Q_\beta} = \sigma_{Q_\beta}/\mu_{Q_\beta}$. For comparison, Fig. 7(a) shows the mean of the stochastic capacity normalised by the deterministic capacity, $Q_{\beta,det}$. It is clear that after initial oscillations both the mean and COV converge to a relatively constant value. Similar convergence was observed for higher moments (skewness and kurtosis), so it is reasonable to assume that the response PDF has been well-captured by the Monte Carlo simulations.

In addition, bootstrap resampling can be used to estimate confidence bounds for statistics derived from a limited number of observations of an unknown PDF [24]. The method involves randomly drawing, with replacement, a set of 'bootstrap' samples from the set of observations and empirically constructing a confidence interval. Here, 95% confidence intervals are generated by the bootstrap method with 10,000 samples.

Table 1 shows the values of mean and standard deviation of $Q_\beta$ at each load inclination, together with the associated bootstrap confidence intervals. The mean stochastic capacity is always less than the deterministic, by 2-3%. One factor that may influence this result is that in a spatially variable soil the caisson is likely to rotate a small amount when subject to loading whereas the deterministic model is set up so as to prevent rotation. The 95% confidence intervals bracket the statistics very closely, indicating a high level of certainty may be placed in the reported values. The COV shows that the variability is very similar around the failure envelope.

### *3.2. Probabilistic failure envelopes*

A description of the stochastic response of the suction caisson using mean and standard deviation does not allow for a straightforward design interpretation; it would be of more use to compare known design loads with a failure envelope associated with a known level of risk, such as the probability that the failure load will fall inside that envelope. Probabilistic failure envelopes were first constructed by Cassidy et al. [27] for strip footings by ranking clusters of failure points and using an empirical estimate of the probability of occurrence.

Here, probabilistic failure envelopes can be defined by observing that the ultimate capacity at each loading angle $\beta$ is a random variable, denoted $Q_\beta$ as before. The Monte Carlo simulations produce samples from the unknown PDF of each load probe. The probabilistic envelopes are then constructed directly from the CDF of each random variable, $F_{Q_\beta}$. It is necessary to obtain a capacity $F_{Q_{\beta,p}}$ such that for a given probability $p$:

$$p = F_{Q_\beta}(Q_{\beta,p}) = P(Q_\beta \leq Q_{\beta,p}) \tag{12}$$

If $\mathbf{Q}$ is the collection of random variables $Q_\beta$, i.e. $\mathbf{Q} = \{Q_0, Q_{30}, \cdots, Q_{90}\}$, the probabilistic VH failure envelope $\mathbf{Q}_p$ is constructed componentwise by:

$$Q_{\beta,p} = F^{-1}_{Q_\beta}(p) \tag{13}$$

with each $Q_{\beta,p}$ consisting of horizontal and vertical load components, $\mathrm{H}_{\beta,p}$ and $\mathrm{V}_{\beta,p}$. The probabilistic failure envelope corresponding to $p$ is therefore the envelope on which there is a probability p that the ultimate capacity of the suction caisson will occur on or inside that envelope. In practice a suitable value of $p$ might then be a low quantile, such as 5%, which would be in line with recommendations for characteristic values of resistance parameters in, for example, Eurocode 7 [28] and the offshore design guidance document DNV-RP-C207 [29].

Kernel density estimation (KDE) is used to obtain the CDFs in each loading direction. The robust and optimal KDE method of Botev et al. [30] is applied. A non-parametric technique is appropriate as it avoids the need to assume a response distribution, which may be different in each loading direction. The advantage of using a KDE-derived CDF rather than the empirical version is that the CDF must be a continuous and strictly increasing function in order to obtain unique values of $Q_{\beta,p}$ from Eq. (13). These conditions are not satisfied by the empirical CDF, as shown in Fig. 8. This is particularly true at the tails of the distribution, which are likely to be of practical interest. No closed-form solution is available for the estimated CDF and so Eq.

(13) is solved by evaluating values of the CDF on a fine one-dimensional grid (at 4096 points in this case) and using interpolation if required.

Fig. 9 shows probabilistic VH failure envelopes for the isotropic autocorrelation $L_x = L_y =$ 1m. It can be seen that the probabilistic envelopes have a similar shape to the deterministic case, which is to be expected considering the relative uniformity of shape observed in Fig. 6. The 50% envelope represents the median, and at all points is inside the deterministic envelope by 2-3%. It can be seen that the deterministic envelope is very close to the 75% envelope, meaning there is a probability of approximately 75% that the holding capacity of the caisson will be less than or equal to the deterministic capacity if the spatial variation of $s_u$ is considered. This illustrates the importance of including the inherent spatial variability of soil properties in the design process.

### *3.3. Effect of autocorrelation distance*

Phoon and Kulhawy [22] reported that there is a relatively limited amount of information available in literature on the autocorrelation structure of soil parameters when compared to other statistical properties, and this remains the case today. In particular there is a lack of data on horizontal correlation, most likely due to the fact that correlation in the vertical distance may be computed based on standard site investigation techniques such as cone penetration tests. It has also been noted that the sampling plan will affect autocorrelation distances [23], bringing into question the validity of reported values.

This leads to the conclusion that in a typical design scenario the inherent variability of a soil, described by its second order statistics, can be reasonably well characterised but the autocorrelation distances may be less well known and may have to be assumed. A study of the effects of autocorrelation distance on the holding capacity of suction caissons has therefore been conducted. The autocorrelation function is assumed exponential, as defined by Eq. (8). In view of the convergence observed in Fig. 7, for cases other than $L_x = L_y =$ 1m 500 Monte Carlo simulations were used to characterise the stochastic response; this allowed a wide-ranging study of autocorrelation distances to be undertaken. The bootstrap method is again used to construct 95% confidence intervals.

#### *3.3.1. Isotropic autocorrelation*

Four isotropic correlation distances have been considered: $L_x = L_y =$ 1, 2, 5, and 8m (corresponding to 0.2D, 0.4D, D and 1.6D). The effect of autocorrelation on the uniaxial capacities is presented in Figure 10(a), where it can be seen that the mean stochastic capacity is consistently

less than the deterministic for all isotropic autocorrelation distances studied. The difference between deterministic and stochastic capacities is greater under vertical loading, but a correspondence is generally observed between the increase or decrease of $\mu_H$ and $\mu_V$. It is notable that the minimum capacity occurs when $L_x = L_y \leq$ D (5m). This is perhaps comparable to the observation that the mean undrained bearing capacity of a strip footing is at a minimum when $L_x$ and $L_y$ are less than or equal to B, the footing width [11], and also noticed in studies of drained bearing capacity [e.g. 31].

Fig. 10(b) shows that as the isotropic autocorrelation distance increases there is a corresponding increase in the COV of $H^*$ and $V^*$ capacities. This is likely to be due to the fact that for short autocorrelations, capacity is dependent on a spatial average over the failure zone due to the rapidly fluctuating areas of low and high strength soil. Conversely, for longer correlation distances, the failure zone may include large areas of strong or weak soil as illustrated in Fig. 5, resulting in greater variability.

In addition, it can be seen that the COV of vertical capacity is greater than for horizontal loading, particularly for longer autocorrelation distances. This may be due to the different failure mechanisms for the two loading cases. Fig. 11 shows the failure mechanisms for horizontal and vertical loading in the deterministic case and two stochastic cases. The distribution of $s_u$ in each model corresponds to the realisations shown in Fig. 5. Under horizontal loading, the failure mechanisms are similar in the deterministic model and in the two stochastic cases shown here, with only minor variations in the path taken by the shear plane. In contrast, when subjected to a vertical load the caisson fails through a symmetric reverse-end bearing mechanism in the deterministic model but in the stochastic cases it can be seen that the failure is non-symmetric. As particularly evident in Fig. 11 for the case of anisotropic autocorrelation ($L_x$ = 10m, $L_y$ = 1m), the failure is governed by a shear plane on just one side, and the caisson rotates as it displaces. The failure mechanism under vertical loading therefore appears to have a much greater scope for variability compared to the horizontal case.

The implication for suction caisson design is more clearly seen by plotting the VH failure envelopes for each autocorrelation distance, as shown in Fig. 12. The zone where the failure envelope can potentially fall is indicated by the position of the 1% and 99% envelopes. This zone widens significantly as $L_x$ and $L_y$ increase. For $L_x = L_y \geq$ 5m, the failure envelope could be reduced in size by as much as 20% compared to a deterministic analysis. For a given design load with a defined PDF, the consequence is that the probability of failure will increase as the potential failure zone widens.

The probabilistic envelopes are very similar in shape across all autocorrelation distances.

Similarly, the envelopes tend to be equally spaced around the median (the 50% envelope), suggesting that each percentile increment corresponds to an approximately equal increase in capacity. It is notable that the probability that the real failure envelope will occur on or inside the deterministic envelope actually reduces as the isotropic autocorrelation distance increases

### *3.3.2. Anisotropic autocorrelation*

The autocorrelation distance of soil properties in the horizontal direction is likely to be greater than in the vertical direction. Values reported in literature suggest the difference is generally an order of magnitude [18]. To observe the effect of anisotropic autocorrelation of undrained shear strength on the VH capacity of a suction caisson the vertical autocorrelation was fixed at 1m (0.2D) and the horizontal autocorrelation varied from 10 to 40m (2D to 8D).

The results for uniaxial loading are shown in Fig. 13. As for the isotropic cases, the mean capacity is lower than the deterministic, with a greater difference between mean and deterministic capacity being observed when loading is in the vertical direction. As the horizontal autocorrelation distance is extended from 10 to 20m there is a slight increase in the mean capacity. However, beyond 20m the mean capacity remains essentially constant. the COV of both $H^*$ and $V^*$ capacity tends to increase with horizontal autocorrelation distance and the COV of vertical capacity is again higher than in the horizontal case. Overall, it is more difficult to identify a clear relationship between the horizontal autocorrelation distance and the statistics of the uniaxial caisson capacity than for the isotropic autocorrelations, when the vertical autocorrelation distance is also changed.

Probabilistic VH failure envelopes for the anisotropic autocorrelation cases are presented in Fig. 14. The size and shape of the 1% and 99% envelopes are broadly similar across the values of $L_x$ considered, the zone of potential failure widening only marginally as $L_x$ increases. This is compared with the large differences observed if $L_x = L_y$ (Fig. 12), and suggests that the vertical autocorrelation distance, $L_y$, has more influence on the variance of the failure envelope than the horizontal. The general profile of shear strength increasing with depth may be disrupted by longer vertical autocorrelations, allowing areas of high or low strength soil to permeate vertically through the soil mass. The vertical autocorrelation distance is therefore of great importance if an envelope associated with a low probability of occurrence must be identified for design.

## 4. Conclusions

A probabilistic analysis of the combined VH capacity of a suction caisson in a normally consolidated undrained clay has been undertaken. The inherent spatial variation of undrained shear strength and the increasing strength with depth that characterise normally consolidated marine deposits are modelled by a random field. This is combined with a deterministic finite element analysis without modification to the finite element code beyond a mapping of the values of random soil parameters. The failure mechanism is therefore a direct result of the random field distribution of undrained shear strength.

VH failure envelopes were produced by loading the suction caisson through a range of angles and Monte Carlo simulation has been used to characterise the probabilistic response. Since this response is unknown prior to analysis, a non-parametric approach was adopted and the method outlined is therefore applicable to any scenario. By using kernel density estimation, probabilistic VH failure envelopes may be produced by inverting the CDF at each loading angle. This enables construction of probabilistic failure envelopes that correspond to the probability, p, that the combination of vertical and horizontal loads that cause failure, $Q_\beta$, is less than or equal to $Q_{\beta,p}$, i.e. $p = P(Q_\beta \leq Q_{\beta,p})$. An appropriate envelope, associated with a clear level of risk, can then be selected for use in design.

A study of the effects of the autocorrelation distance of undrained shear strength has shown that the mean probabilistic capacity remains lower than the deterministic capacity regardless of autocorrelation distance. The variability of the holding capacity increases with the autocorrelation distance, in both isotropic and anisotropic cases. Importantly, the vertical autocorrelation distance has a much greater influence on the variability of the VH response than the horizontal distance. Therefore the value of $L_y$ must be chosen carefully if this procedure is used to construct probabilistic VH failure envelopes.

**Acknowledgements** The first author is funded by a studentship jointly provided by the Engineering and Physical Sciences Research Council (EPSRC) and Atkins. This support is gratefully acknowledged.

[1] Randolph MF, Gaudin C, Gourvenec SM, White DJ, Boylan N, Cassidy MJ. Recent advances in offshore geotechnics for deep water oil and gas developments. Ocean Eng 2011; 38(7): 818-834.

[2] Randolph MF, Cassidy MJ, Gourvenec S, Erbrich C. Challenges of offshore geotechnical engineering. In: Proc 16th Int Conf on Soil Mech and Geotechn Eng, Osaka, Japan, 2005: 123-176.

[3] Zdravkovic L, Potts DM, Jardine RJ. A parametric study of the pull-out capacity of bucket foundations in soft clay. Géotechnique 2001; 51(1): 55-67.

[4] Supachawarote C, Randolph MF, Gourvenec S. Inclined pull-out capacity of suction caissons. In: Proc of the 14th Int Offshore and Polar Eng Conf ISOPE, Toulon, France, 2004:500-506.

[5] Randolph MF, House AR. Analysis of suction caisson capacity in clay. In: Proc of the 34th Ann Int Offshore Tech Conf 2002; Paper No 14236.

[6] Aubeny CP, Han SW, Murff JD. Suction caisson capacity in anisotropic, purely cohesive soil. Int J of Geomech 2003; 3(2): 225-235.

[7] Vásquez LF, Maniar DR, Tassoulas JL. Installation and axial pullout of suction caissons: Numerical modeling. J Geotech Geoenviron Eng 2010; 136(8):1137-1147.

[8] Clukey EC, Banon H, Kulhawy FH. Reliability assessment of deepwater suction caissons. In: Proce Offshore Tech Conf 2000; Paper No. 12192.

[9] Dahlberg R, Ronold KO, Strom PJ, Mathisen J, Andersen KH, Jostad HP. Calibrated geotechnical design code for suction anchors in clay. In: Proce Offshore Tech Conf 2006; Paper No. 18036.

[10] Silva-Gonzàlez F, Heredia-Zavoni E, Valle-Molina C, Sànchez-Moreno J, Gilbert, R.B. Reliability study of suction caissons for catenary and taut-leg mooring systems. Struct Saf 2013; 45:59-70.

[11] Griffiths DV, and Fenton GA. Bearing capacity of spatially random soil: the undrained clay Prandtl problem revisited. Géotechnique 2001;51(4):351-359.

[12] Cho SE. Effects of spatial variability of soil properties on slope stability. Eng Geol 2007; 92(3-4): 97-109.

[13] Ghanem RG, Spanos PD. (2003) Stochastic Finite elements: A spectral approach. 2nd edn. New York: Dover Publications.

[14] Vanmarcke E. Random Fields: Analysis and Synthesis. World Scientific, 2010.

[15] Wroth CP, Houlsby GT. Soil Mechanics - Property characterization and analysis procedures. Keynote lecture. In: Proc 11th Int Conf on Soil Mech and Found Eng (ICSMFE), San Francisco, 1985: 1-55.

[16] Li D-Q, Qi X-H, Phoon K-K, Zhang L-M. Zhou C-B. Effect of spatially variable shear strength parameters with linearly increasing mean trend on reliability of infinite slopes. Struct Saf 2014;49:45-55.

[17] Lumb P. The Variability of Natural Soils. Can Geotech J 1996; 3(2):74-97.

[18] Lacasse S, Nadim F. Uncertainties in characterising soil properties. Uncertainty in the geologic environment: from Theory to Practice. New York: ASCE, 1996; 49-75.

[19] Wu S-H, Ou C-Y, Ching J, Juang CH. Reliability-based design forbasalheave stability of deep excavations in spatially varying soils. J Geotech Geoenviron Eng 2012;138(5):594-603.

[20] Andresen L, Edgers L, Jostad HP. Capacity analysis of suction anchors in clay by Plaxis 3D foundation. Plaxis Bulletin 2008; (24): 5-9.

[21] Andersen KH, Murff JD, Randolph MF, Clukey EC, Erbrich C, Jostad HP, Hansen B, Aubeny CP, Sharma P, Supachawarote C. Suction anchors for deepwater applications. In Proc Int Symposium on Frontiers in Offshore Geotechnics (ISFOG), Perth, Western Australia Balkema 2005: 3-30.

[22] Phoon KK, Kulhawy FH. Characterization of geotechnical variability. Can Geotech J 1999;36(4):612-624.

[23] DeGroot DJ, Baecher GB. Estimating autocovariance of in-situ soil properties. J of Geotech Eng 1993; 119(1):147-166.

[24] Efron B. Bootstrap methods: another look at the jackknife. Ann of Stat 1979; 38(5):1-26.

[25] Plaxis 2D. Delft, Netherlands 2012; Plaxis bv.

[26] Andersen KH, Jostad HP. Shear strength along outside wall of suction anchors in clay after installation. In: Proc 12th Int Offshore and Polar Engng Conf, Kitakyushu, Japan 2002: 785-794.

[27] Cassidy MJ, Uzielli M, Tian, Y. Probabilistic combined loading failure envelopes of a strip footing on spatially variable soil. Comput and Geotech 2013; (49): 191-205.

[28] EC7-1 Eurocode 7: Geotechnical design Part 1: General rules, London, British Standards Institution, 2004:BS EN 1997-1.

[29] DNV-RP-C207: Statistical Representation of Soil Data. Norway: Det Norske Veritas, 2012.

[30] Botev ZI, Grotowski JF, Kroese DP. Kernel density estimation via diffusion. Ann Stat 2010;38(5): 2916-2957.

[31] Al-Bittar T, Soubra AH. Bearing capacity of strip footings on spatially random soils using sparse polynomial chaos expansion. Int J Numer Anal Methods Geomech 2013;37(13):2039-2060.

[32] Ahn J, Lee H, Kim Y-T. Holding capacity of suction caisson anchors embedded in cohesive soils based on finite element analysis. Int J Numer Anal Methods Geomech 2014; 38(15):1541-1555.

[33] Senders M, Kay S. Geotechnical suction pile anchor design in deep water soft clays. In: Proc 7th Annual Deepwater Risers, Moorings and Anchorings Conf, IBC, London, 2002: 50.

[34] Zdravkovic L, Potts DM, Jardine RJ. Pull-out capacity of bucket foundations in soft clay offshore site investigation and foundation behaviour. In: Proc Int Offshore Site Investigation and Found Behaviour Conf, SUT, London, 1998: 301-324.

**List of Figures**

**List of Tables**

Table 1: Deterministic and stochastic ultimate capacity at each loading angle. For stochastic analyses, 95% confidence intervals (CI) of mean ($\mu$) and standard deviation ($\sigma$) are shown. COV = Coefficient of Variation.

| $\beta$ | Deterministic | $\mu$ | 95% $CI$ | $\sigma$ | 95% $CI$ | COV |
|---|---|---|---|---|---|---|
| ($^o$) | (kN/m) | (kN/m) | (kN/m) | (kN/m) | (kN/m) | |
| 0 | 229.9 | 225.3 | (224.88, 225.81) | 7.57 | (7.27, 7.89) | 0.034 |
| 30 | 265.2 | 258.8 | (258.20, 259.28) | 8.83 | (8.45, 9.23) | 0.034 |
| 45 | 309.6 | 302.0 | (301.36, 302.72) | 10.56 | (10.18, 11.05) | 0.035 |
| 60 | 356.7 | 348.7 | (347.92, 349.45) | 12.74 | (12.24, 13.26) | 0.037 |
| 75 | 406.3 | 396.9 | (395.96, 397.80) | 14.73 | (14.13, 15.41) | 0.037 |
| 90 | 446.2 | 430.3 | (429.35, 431.26) | 14.94 | (14.36, 15.56) | 0.035 |

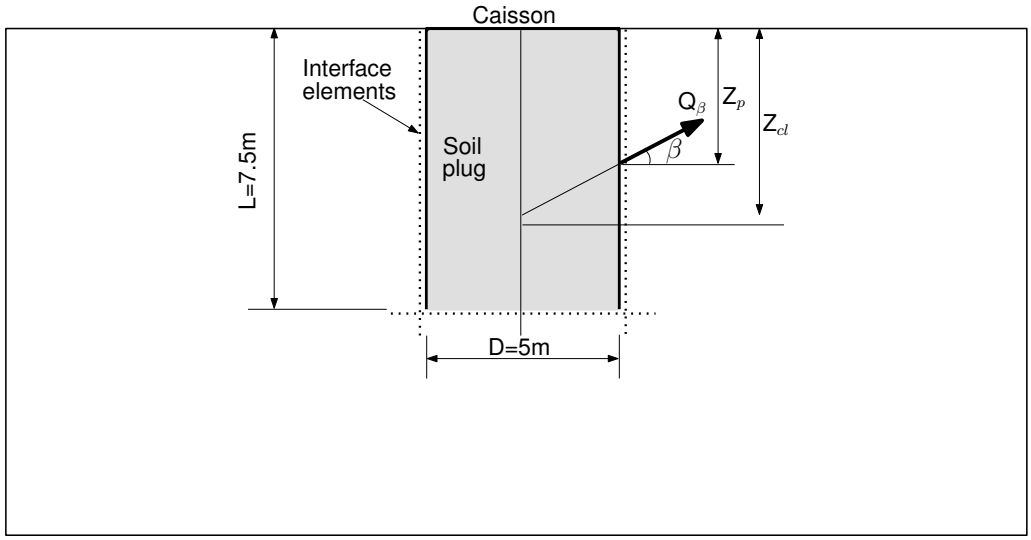


Figure 1: Layout of the suction caisson.

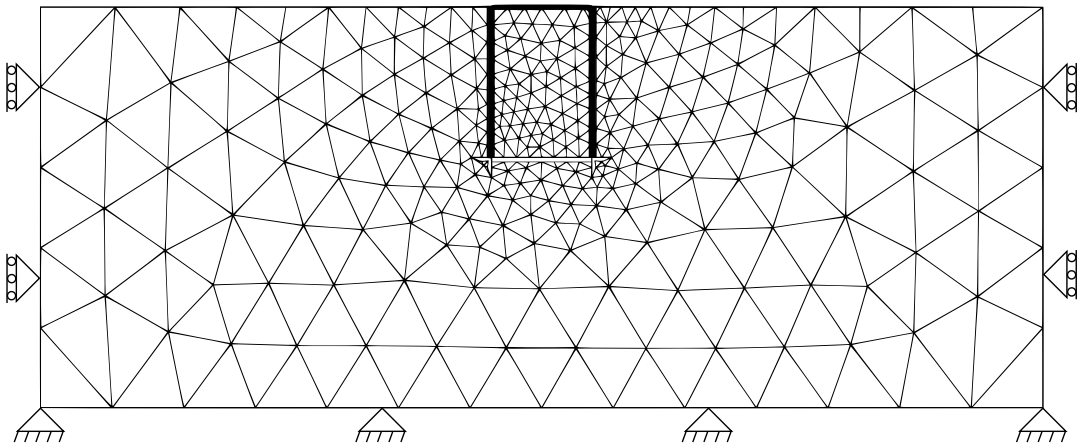

Figure 2: Finite element mesh.

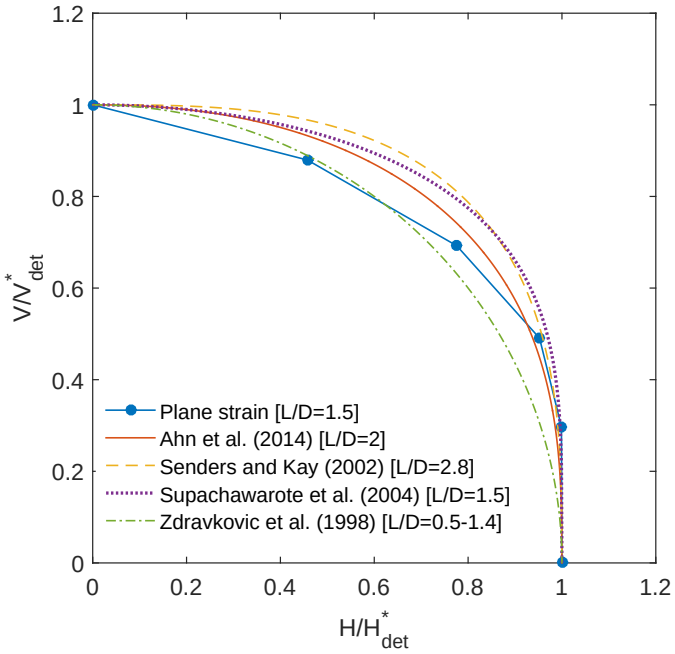


Figure 3: Normalised deterministic failure envelope: comparison between plane strain results and closed-form expressions [32, 33, 4, 34].

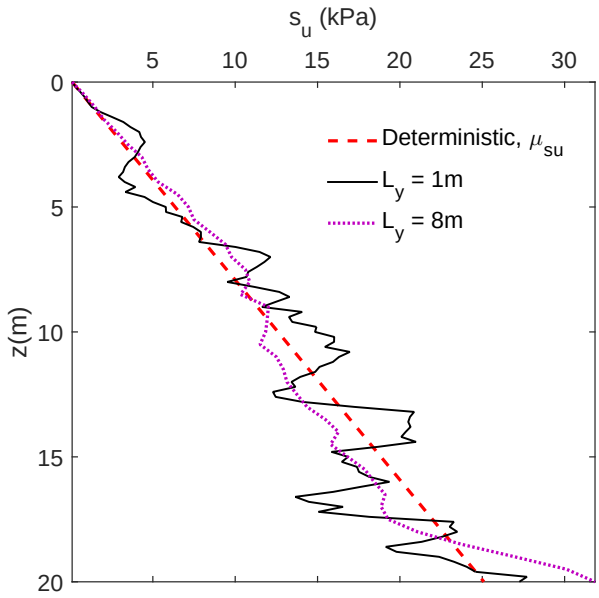


Figure 4: Increase in undrained shear strength with depth in deterministic case and for realisations of random fields with $L_y = 1$m and $L_y = 8$m.

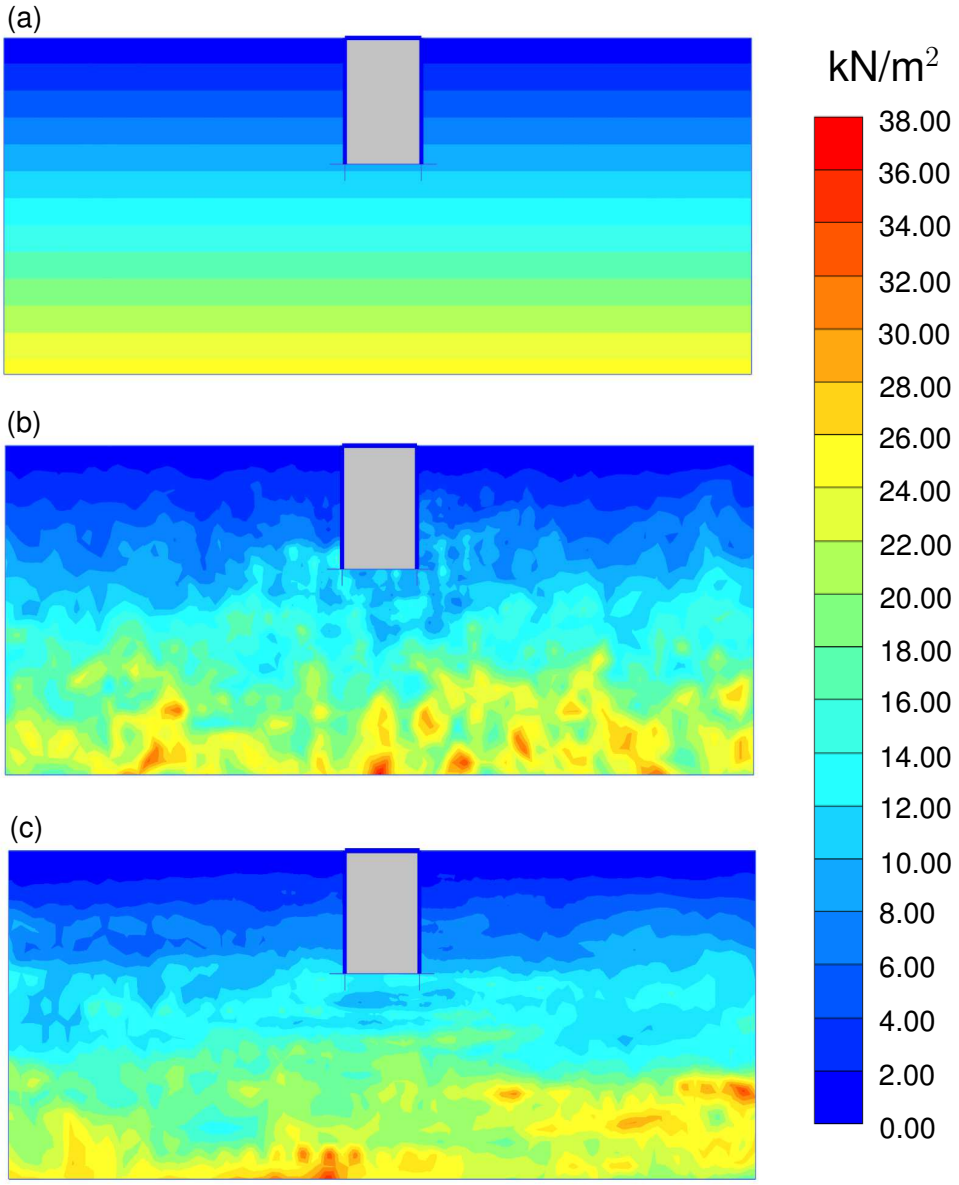


Figure 5: Distribution of $s_u$ in the finite element model: (a) Deterministic; (b) Random field realisation with autocorrelation distances $L_x = L_y = 1$m; (c) Random field realisation with autocorrelation distances $L_x = 10$m, $L_y = 1$m.

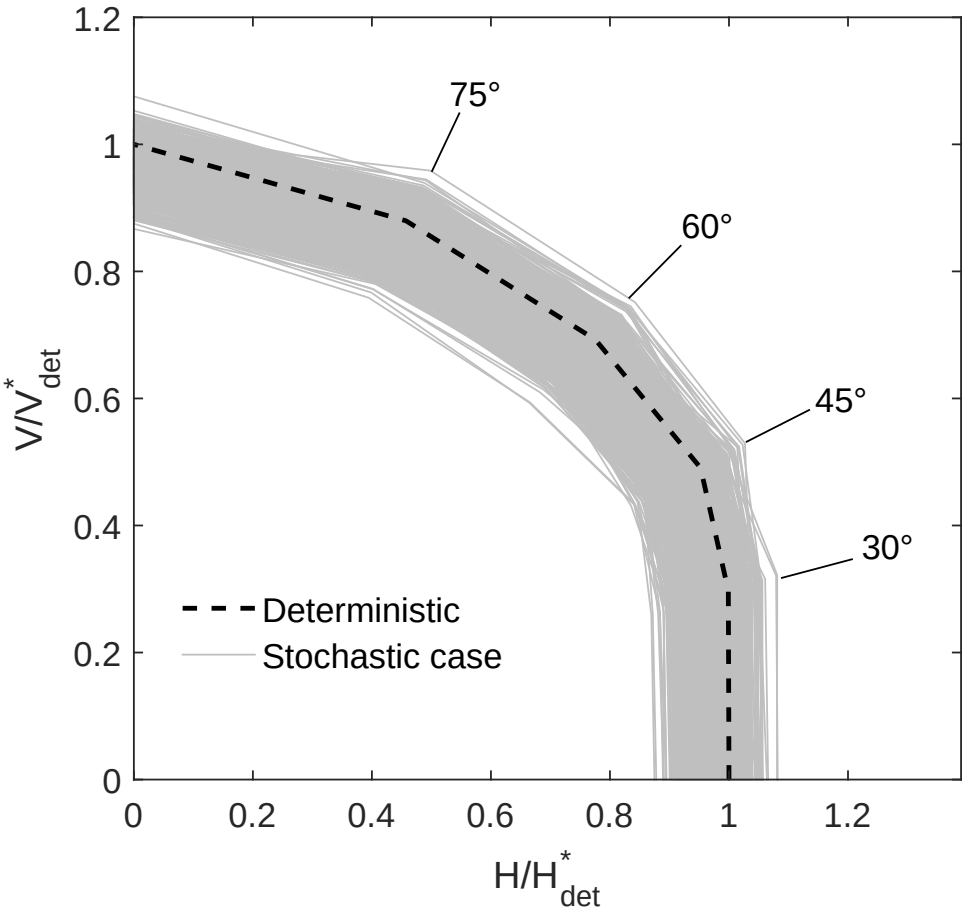


Figure 6: Stochastic and deterministic VH failure envelopes (1000 simulations). Loading angles are also indicated.

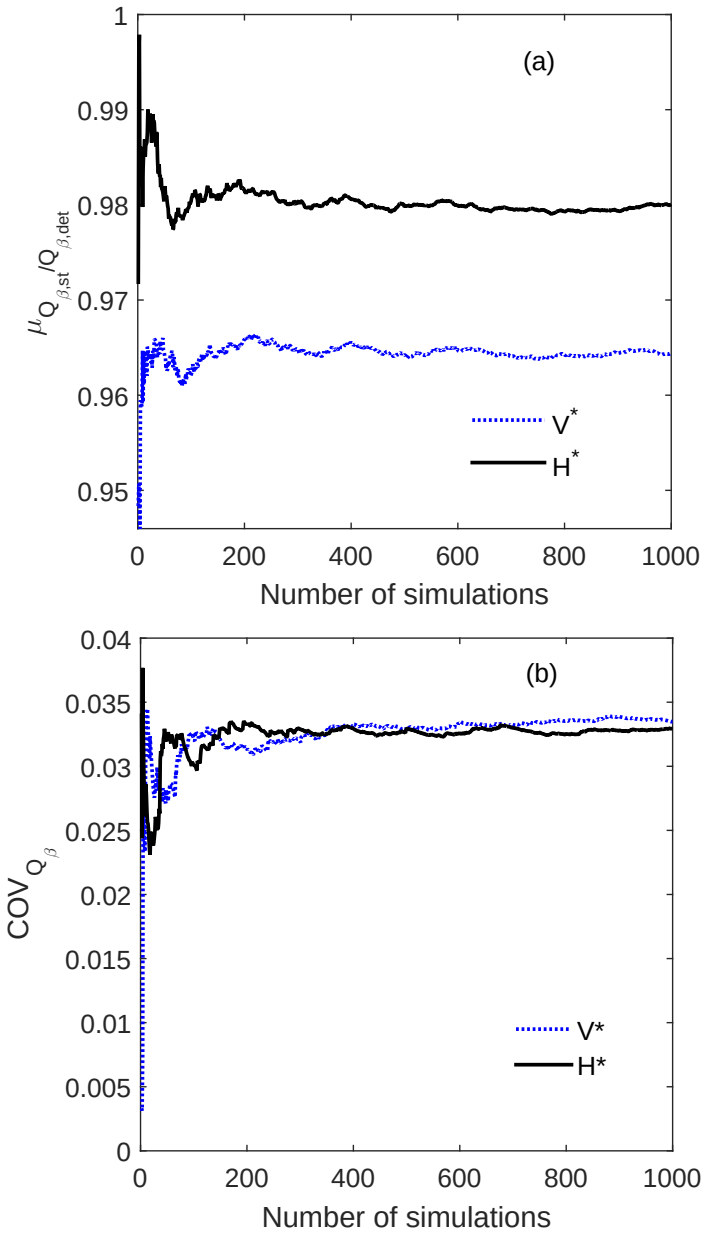


Figure 7: Normalised stochastic capacity: Mean of normalised uniaxial capacities $V^*$ and $H^*$ and (b) COV of $V^*$ and $H^*$ as a function of number of Monte Carlo simulations.

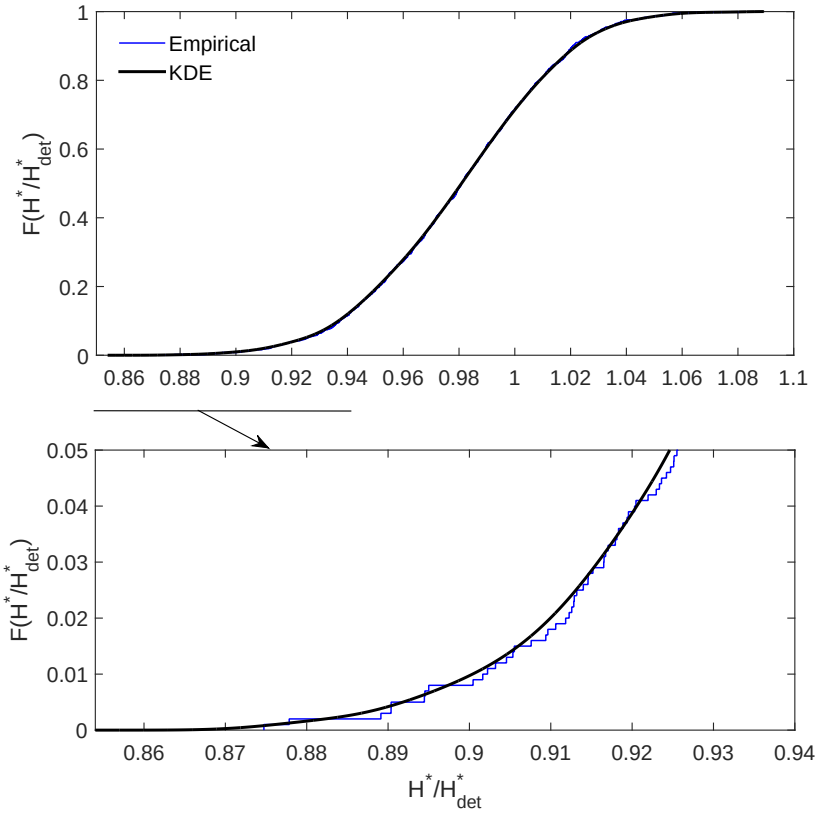


Figure 8: Empirical and KDE-derived CDF of normalised horizontal capacity.

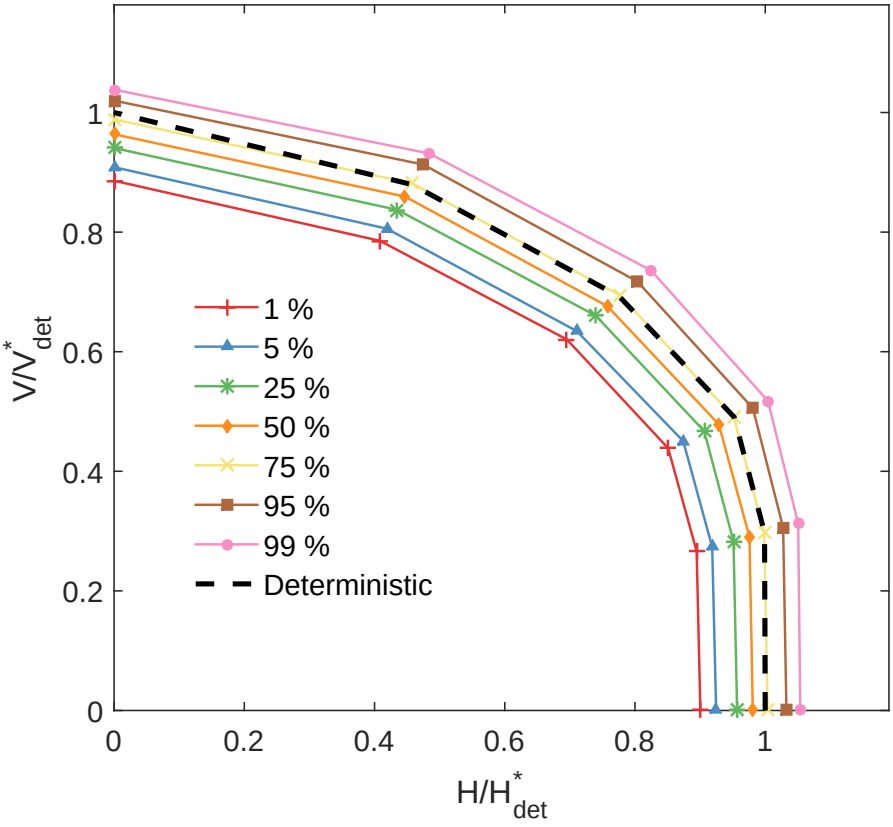


Figure 9: Probabilistic VH failure envelopes.

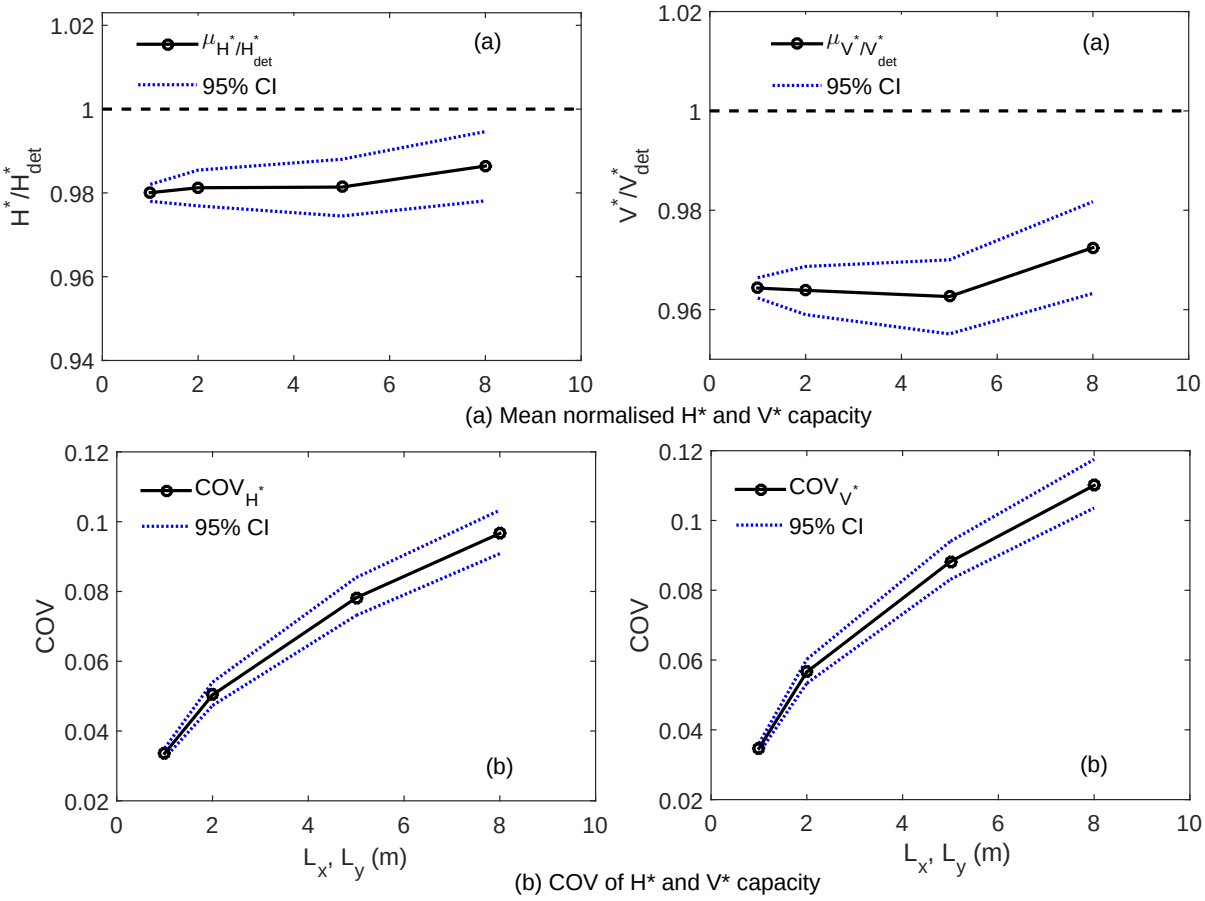


Figure 10: Effect of autocorrelation distance on uniaxial horizontal ($H^*$) and vertical ($V^*$) (a) mean normalised $H^*$ and $V^*$ capacity and (b) COV of $H^*$ and $V^*$ capacity.

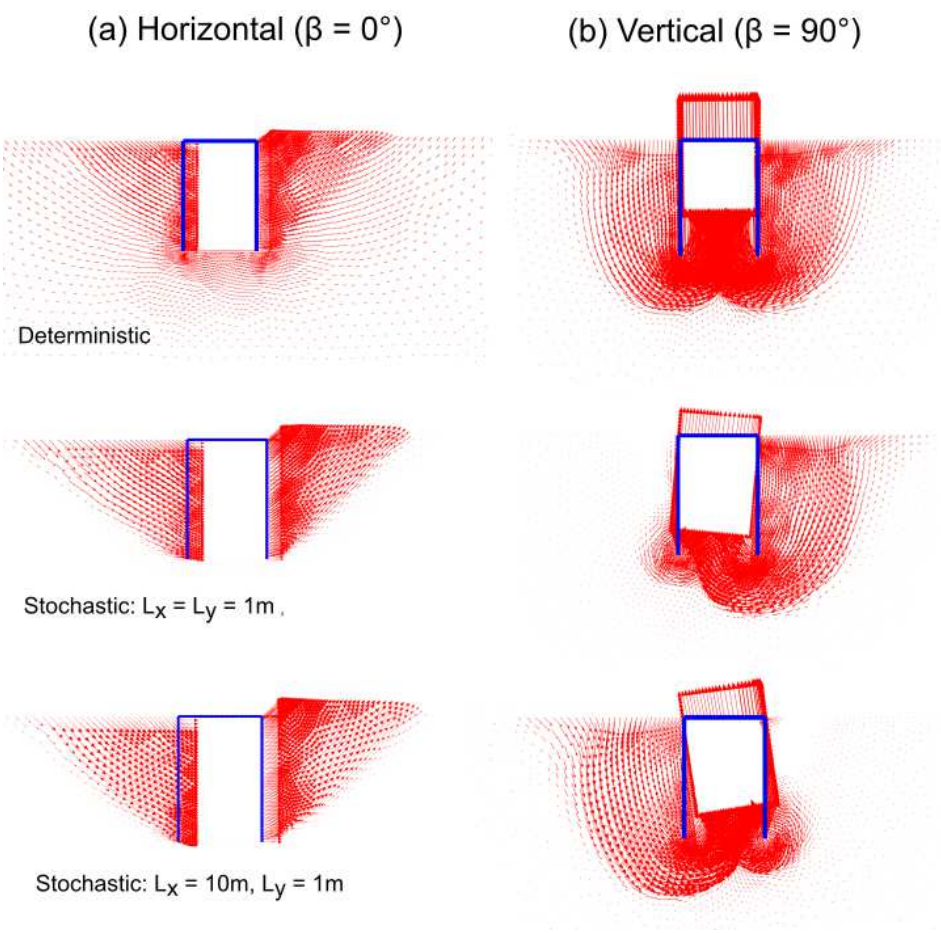


Figure 11: Displacement vectors at failure for (a) Horizontal loading ($H^*$) and (b) Vertical loading ($V^*$). For stochastic cases, the random field realisations correspond to Fig. 5.

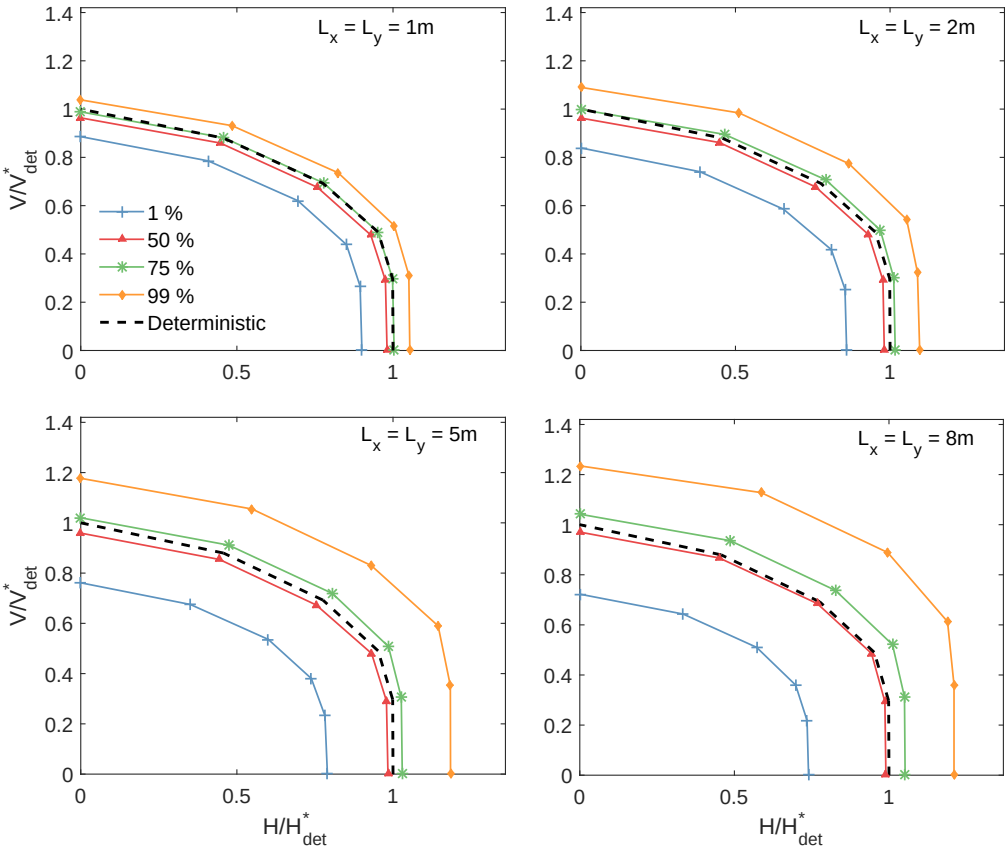


Figure 12: Probabilistic VH failure envelopes for different isotropic autocorrelation distances.

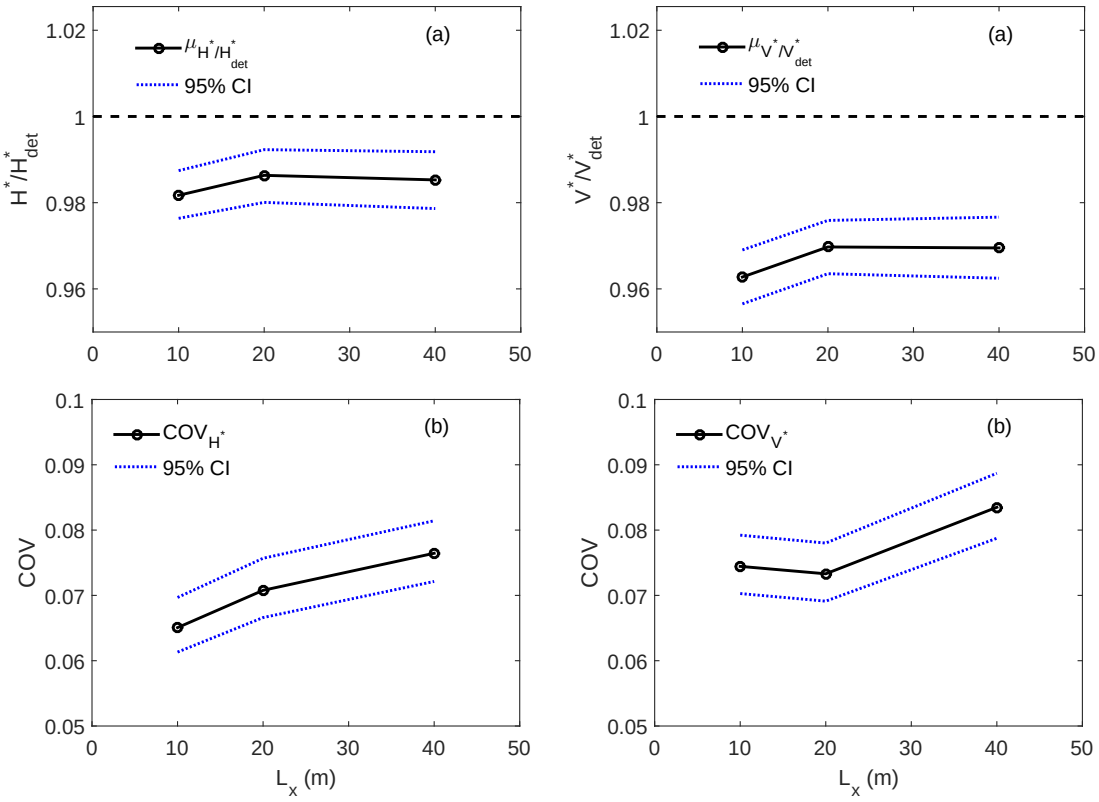


Figure 13: Effect of horizontal autocorrelation distance on uniaxial horizontal and vertical (a) mean capacity and (b) COV. $L_y$ = 1m.

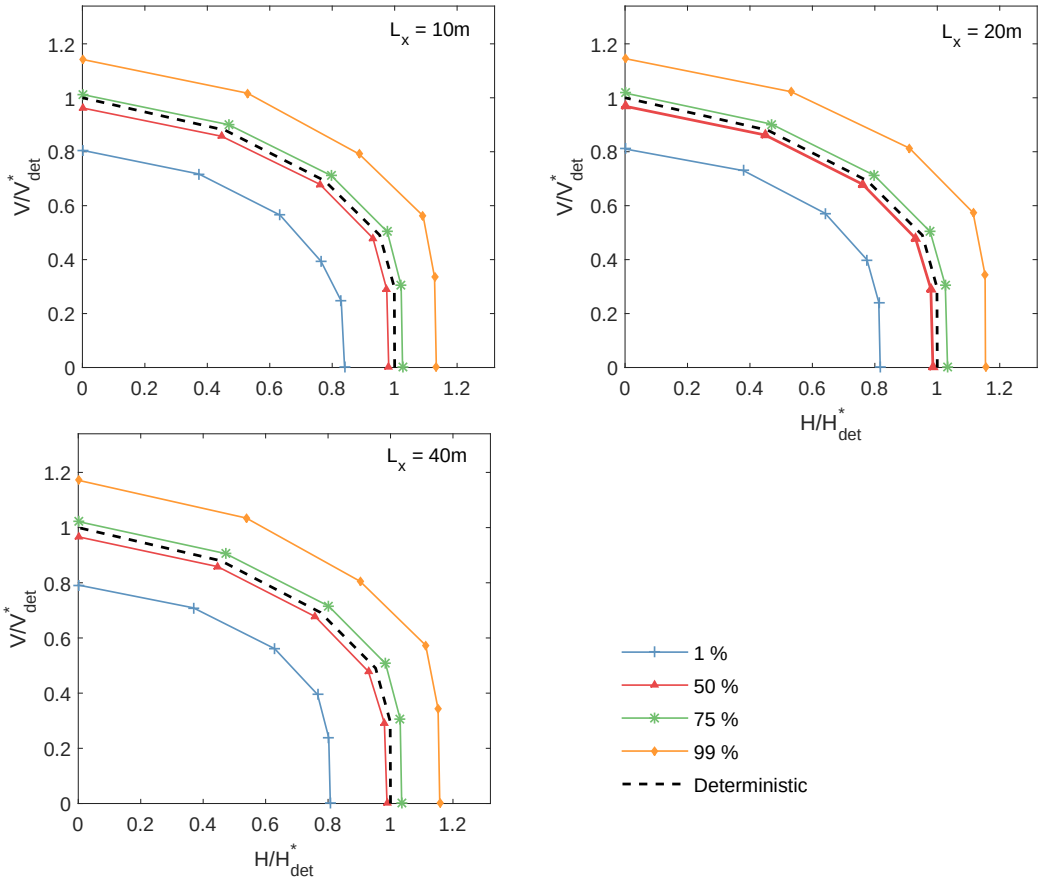


Figure 14: Probabilistic VH failure envelopes for anisotropic autocorrelation. $L_y$ = 1m.